environmental sciences proceedings

MDPI

Proceeding Paper

Assessment of Satellite and Reanalysis Precipitation Products for Rainfall–Runoff Modelling in a Mountainous Basin †

Hamed Hafizi [1,2] and Ali Arda Sorman [1,*]

[1] Department of Civil Engineering, Eskisehir Technical University, Eskisehir 26555, Turkey; hamedhafizi@eskisehir.edu.tr
[2] Department of Hydraulics and Hydraulic Structures, Faculty of Water Resources and Environmental Engineering, Kabul Polytechnic University, Kabul 1010, Afghanistan
* Correspondence: asorman@eskisehir.edu.tr
† Presented at the 4th International Electronic Conference on Atmospheric Sciences, 16–31 July 2021; Available online: https://ecas2021.sciforum.net/.

Abstract: Precipitation measurement over a complex topography and highly elevated regions has always been a great challenge in recent decades. On the other hand, satellite-based and numerical weather prediction model outputs can be an alternative to fill this gap. Hence, the goal of this study is to evaluate the spatiotemporal stability and hydrologic utility of four precipitation products (TMPA-3B42v7, IMERGHHFv06, ERA5, and PERSIANN) over a mountainous basin (Karasu basin) located in the eastern part of Turkey. Moreover, the Kling–Gupta efficiency (KGE), including its correlation, bias, and variability ratio components, are used for a direct comparison of precipitation products (PPs) with observed gauge data, and the Hansen–Kuiper (HK) score is utilized to assess the detectability strength of PPs for different precipitation events. In the same way, the hydrologic utility of PPs is tested by exploiting a conceptual rainfall–runoff model under Kling–Gupta efficiency (KGE) and Nash–Sutcliffe efficiency (NSE) metrics. Generally, all PPs show low performance for a direct comparison with observed data while their performance considerably increases for streamflow simulation. TMPA-3B42v7 has high reproducibility in streamflow (KGE = 0.84), followed by IMERGHHFv06 (KGE = 0.76), ERA5 (KGE = 0.75), and PERSIANN (KGE = 0.70), for the entire period (2015–2019) of this study.

Keywords: precipitation products; validation; rainfall–runoff modeling; mountainous basin; Turkey

check for updates

Citation: Hafizi, H.; Sorman, A.A. Assessment of Satellite and Reanalysis Precipitation Products for Rainfall–Runoff Modelling in a Mountainous Basin. *Environ. Sci. Proc.* **2021**, *8*, 25. https://doi.org/10.3390/ecas2021-10345

Academic Editor: Anthony R. Lupo

Published: 22 June 2021

Publisher's Note: MDPI stays neutral with regard to jurisdictional claims in published maps and institutional affiliations.

Copyright: © 2021 by the authors. Licensee MDPI, Basel, Switzerland. This article is an open access article distributed under the terms and conditions of the Creative Commons Attribution (CC BY) license (https://creativecommons.org/licenses/by/4.0/).

1. Introduction

High spatial and temporal resolution precipitation estimates are essential for dealing with problems related to water resources management, flood forecasting, agricultural forecasts, and natural hazards [1,2]. Moreover, utilizing hydrologic models for rainfall–runoff simulation in a basin always needs accurate precipitation estimates, which are limited for most regions [3]. Precipitation estimation by a rain gauge network is one of the well-known methods and provides the opportunity of direct physical measurement of precipitation with high accuracy above the ground level [4,5]. However, rain gauges are limited over time and space, and usually, the network is denser in low-lying areas. Highland regions, which typically have a complex topography, suffer from gauge scarcity, which causes detrimental effects in rainfall–runoff simulations over mountainous basins [6–9].

In recent years, precipitation derived from satellites using passive microwave (PMW) and infrared (IR) sensor information and numerical weather prediction model outputs can be an alternative in poorly gauged regions around the world. Hence, satellite and reanalysis precipitation products (PPs) have been implemented for numerous hydrometeorological studies, such as rainfall–runoff simulation [10], natural hazard [11], climate change [12], and renewable energy [13].

Moreover, a number of precipitation products (PPs) with different spatial and temporal resolutions from various sources have been developed, such as Tropical Rainfall Measuring Mission (TRMM) Multisatellite Precipitation Analysis (TMPA) 3B42v7 [14], Integrated Multi-satellitE Retrievals for the Global Precipitation Measurement (GPM) Half Hourly (IMERGHH) final run v06 [15], European Centre for Medium Range Weather Forecasts (ECMWF) reanalysis fifth generation (ERA5) [16], and Precipitation Estimation from Remotely Sensed Information using Artificial Neural Networks (PERSIANN) [17].

Furthermore, the application of hydrologic models has received considerable attention for solving real-world problems related to water resources management and development, and the hydrologic models' structures vary from simple to very sophisticated, considering the level of information used in the model for a particular problem [18–20].

The consistency of different PPs has been carried out by several authors in regional and global scales around the world [21–23]. However, the reliability of PPs over a specific area is not applicable for another region, and an individual assessment is needed to address the stability of PPs. While different studies have been carried out to address the reliability of some PPs over Turkey [24–26], either previous studies considered only direct comparison, excluding the hydrologic utility, or modeling was taken into account in a coarse time step, such as monthly. In this work, we both consider direct PP comparison, including seasonal variability, and utilize PPs in hydrologic modeling in a daily time step.

The aim of this study is to evaluate both the meteorological and the hydrological stability of four PPs (TMPA-3B42v7, IMERGHHFv06, ERA5, and PERSIANN), considering the seasonal variability of precipitation in daily time step for 5 water years from October 2014 to September 2019.

The structure of this paper is as follow: Section 1 presents a comprehensive introduction to PPs. Section 2 of this study gives information on materials and methods. Section 3 presents the results and detailed discussions, and finally, conclusions are conveyed in Section 4.

2. Materials and Methods

2.1. Study Area

With a drainage area of around 10,250 km^2, Karasu River originates the headwaters of the largest basin (Euphrates) in Turkey situated within 38°58′ E to 41°39′ E and 39°23′ N to 40°25′ N. The basin elevation varies from 1130 to 3500 m, and the outlet is controlled by the Kemah Boğazı (E21A019) stream gaging station (Figure 1).

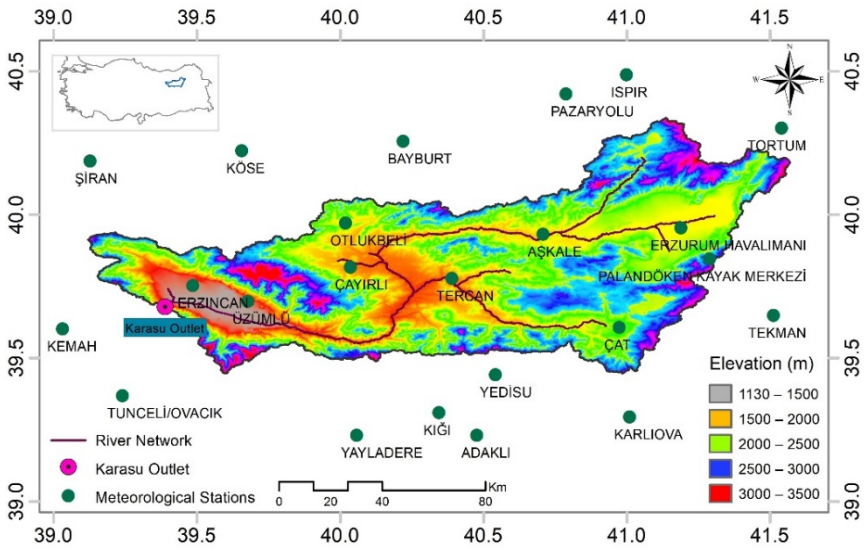

Figure 1. Geographical location, basin elevation (m), meteorological stations, and hydrological station located in the study area.

2.2. Data

In the study, daily precipitation and temperature data from 23 meteorological stations are provided by the General Directorate of Meteorology (GDM), and streamflow data at the basin outlet (E21A019) are obtained from the General Directorate of Hydraulic Works (GDHW) for 5 water years (October 2014 to September 2019). Moreover, daily precipitations from four PPs, TRMM Multisatellite Precipitation Analysis (TMPA) 3B42v7, Integrated Multi-satellitE Retrievals for GPM (IMERG) Half Hourly final run v06, European Centre for Medium Range Weather Forecasts (ECMWF) reanalysis fifth generation (ERA5), and Precipitation Estimation from Remotely Sensed Information using Artificial Neural Networks (PERSIANN), are acquired from different sources for validation. The properties of the selected GPDs are summarized in Table 1.

Table 1. Properties of selected the PPs, abbreviations in the data source column; G, gauge; S, satellite; R; reanalysis.

Name	Data Source(s)	Spatial Resolution	Spatial Coverage	Temporal Resolution	Reference
TMPA-3B42v7	G, S	0.25°	50° N/S	3 hourly	[14]
IMERGHHFv06	G, S	0.10°	60° N/S	30 min	[15]
ERA5	R	0.25°	50° N/S	Hourly	[16]
PERSIANN	S	0.25°	60° N/S	Hourly	[17]

2.3. Methodology

For the direct comparison of PPs with observed precipitation, the Kling–Gupta efficiency (KGE) [27,28], which is a combination of correlation, bias, and variability ratio, is utilized. In the same way, the Hansen–Kuiper (HK) score is used to measure the detectability strength of PPs for five different precipitation categories based on the World Meteorological Organization [29] and modified by Zambrano-Bigiarini [30].

The five precipitation thresholds considered are: no precipitation (less than 1 mm/day), light precipitation (1–5 mm/day), moderate precipitation (5–20 mm/day), heavy precipitation (20–40 mm/day), and violent precipitation (more than 40 mm/day). Moreover, the Nash–Sutcliffe efficiency (NSE) and KGE are selected to evaluate the hydrologic utility of PPs for streamflow simulation. Two scenarios are considered in this case; first, the model parameters are calibrated using observed precipitation by ground stations, and then PPs are replaced and tested individually (scheme-1). Second, the model parameters are calibrated and validated for each PP independently (scheme-2). Table 2 shows the properties of the selected evaluation metrics whereby the optimal value is unity for each of them.

For the hydrologic modeling part, the TUW model, a conceptual hydrologic model developed by the Technical University of Vienna and built based on the similar structure of the HBV model, is utilized, operating at a daily time scale. The TUW model has 15 parameters and is able to simulate runoff, snow, and soil moisture using inputs from daily accumulated precipitation, daily average temperature, and daily potential evapotranspiration. Moreover, for model parameter calibration, the observed streamflow is demanded by the model. Information on 15 model parameters are summarized in Table 3.

Table 2. Properties of the performance indices for the evaluation of PPs.

Performance Indicator	Mathematical Statement	Explanation
Kling–Gupta efficiency and its components	$KGE = 1 - \left[(R - 1)^2 + (\beta - 1)^2 + (VR - 1)^2\right]^{0.5}$ $R = \frac{1}{n}\sum_{1}^{n}(o_n - \mu_0)(s_n - \mu_s)/(\delta_o \times \delta_s)$, $\beta = \frac{\mu_s}{\mu_o}$, $VR = (\delta_s \times \mu_o)/(\mu_s \times \delta_o)$	*R* (*Pearson correlation coefficient*), β (*bias*) is the ratio of the estimated and observed mean, *VR* (*variability ratio*) is the ratio of estimated and observed coefficients of the variation, μ and δ are the distribution mean and standard deviation where *s* and *o* indicate estimated and observed. *M* (*miss*) is when the observed precipitation is not detected. *F* (*false*) is when the precipitation is detected but not observed, *H* (*hit*) is when the observed precipitation is correctly detected, *CN* (*correct negative*) is when no precipitation event is detected. *n* is the sample size of the observed or calculated streamflow. Q_i^{ob} and Q_i^{sim} present the observed and simulated streamflow, and $\overline{Q_i^{ob}}$ presents the mean observed streamflow.
Hansen–Kuiper	$HK = \frac{(H \times CN) - (F \times M)}{(H+M)\ (F+CN)}$	
Nash–Sutcliffe efficiency	$NSE = 1 - \frac{\sum_{i=1}^{n}(Q_i^{sim} - Q_i^{ob})^2}{\sum_{i=1}^{n}(Q_i^{ob} - \overline{Q_i^{ob}})^2}$	

Table 3. Model parameter range and optimum values for observed precipitation and PPs. Number of the column indicates: 0, parameter range; 1, Obs; 2, TMPA-3B42v7; 3, IMERGHHFv06; 4, ERA5; and 5, PERSIANN.

Parameter and Units	0	1	2	3	4	5
Snow correction factor—SCF (-)	0.9–1.5	1.44	1.12	1.03	0.91	1.46
Degree-day factor—DDF (mm/°C/day)	0.0–5.0	0.36	0.3	0.51	0.36	0.33
Temperature threshold above which precipitation is rain—Tr (°C)	1.0–3.0	2.51	1.74	1.43	2.92	2.99
Temperature threshold below which precipitation is snow—Ts (°C)	−3.0–1.0	−1.01	−0.01	−0.1	−2.13	1
Temperature threshold above which melt starts—Tm (°C)	−2.0–2.0	−0.5	−1.86	0.87	−0.92	1.87
Parameter related to the limit for potential evaporation—Lpart (-)	0.0–1.0	0.88	0.6	0.36	0.82	0.69
Field capacity—FC (mm)	0.0–600	132.2	317.8	45.3	115.3	591.5
Nonlinear parameter for runoff production—Beta (-)	0.0–20	0.97	1.82	5.52	14.75	0.05
Constant percolation rate—K_0 (mm/day)	0.0–2.0	0.69	1.09	0.73	1.2	1.34
Storage coefficient for very fast response—K_1 (day)	2.0–30	26.39	23.12	20.06	27	27.08
Storage coefficient for fast response—K_2 (day)	30–250	36.1	38.3	50.9	78.5	245.5
Storage coefficient for slow response—lsuz (day)	1.0–100	51.8	87.9	57.5	46.4	98.4
Threshold storage state—cperc (mm)	0.0–8.0	6.44	5.03	6.97	6.79	0.39
Maximum base at low flows—bmax (day)	0.0–30	14.23	13.65	7.78	7.45	15.4
Free scaling parameter—croute (day^2/mm)	0.0–50	17.81	27.37	24.35	29.37	5.32

3. Result and Discussion

3.1. Mean Daily Precipitation

Figure 2 shows the mean daily precipitation from observed precipitation and four PPs, including their bias over the study area for the entire period (2014–2019) and four seasons. Overall, the region receives 1.5 mm/day precipitation for the entire period, where this amount increases to 2.2 mm/day during the spring and reduces to 0.7 mm/day in the summer. Precipitation during the autumn (1.1 mm/day) is less when compared with that during the winter (1.8 mm/day).

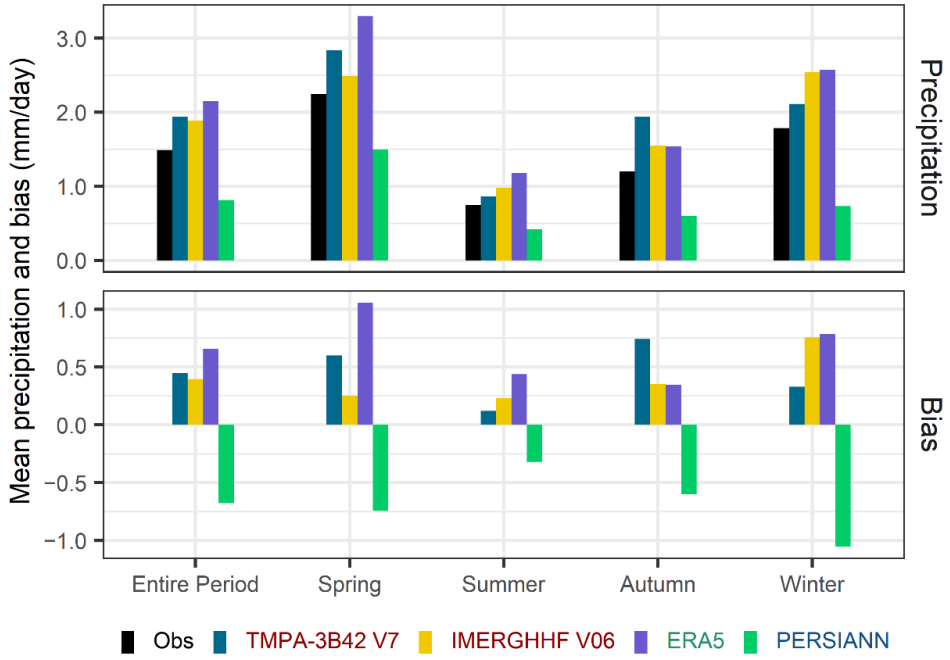

Figure 2. Mean daily precipitation and its bias compared with observed precipitation over the study region for the entire period and four seasons. Legend text color presents: satellite (blue), gauge and satellite (red), Reanalysis (green) and gauge (black).

Furthermore, among all the PPs, PERSIANN always underestimates precipitation, while the others show an overestimation of mean daily precipitation, with ERA5 giving the highest overestimate (bias, 1.1 mm/day) during the spring season. Both IMERGHHFv06 and ERA5 show close mean daily precipitation during the autumn and winter seasons, while TMPA-3B42v7 displays more precipitation (1.9 mm/day) during the autumn season and presents the lowest bias (0.12 mm/day) in the summer, comparatively.

3.2. Quantitative and Categorical Performance of PPs

Figure 3 indicates the median of the Kling–Gupta efficiency (KGE), including its three components for the entire period and four seasons. All PPs perform weakly for daily precipitation in Karasu basin, where the highest performance is given by ERA5 (median KGE, 0.27) during the autumn season. Moreover, among the gauge-corrected PPs, TMPA-3B42v7 shows the highest bias (1.61) over the study area for the entire period, where IMERGHHFv06 significantly overestimates the bias (median of bias, 2.14) during the winter. Furthermore, PERSIANN always underestimates the bias and overestimates the variability ratio for the entire period and four seasons.

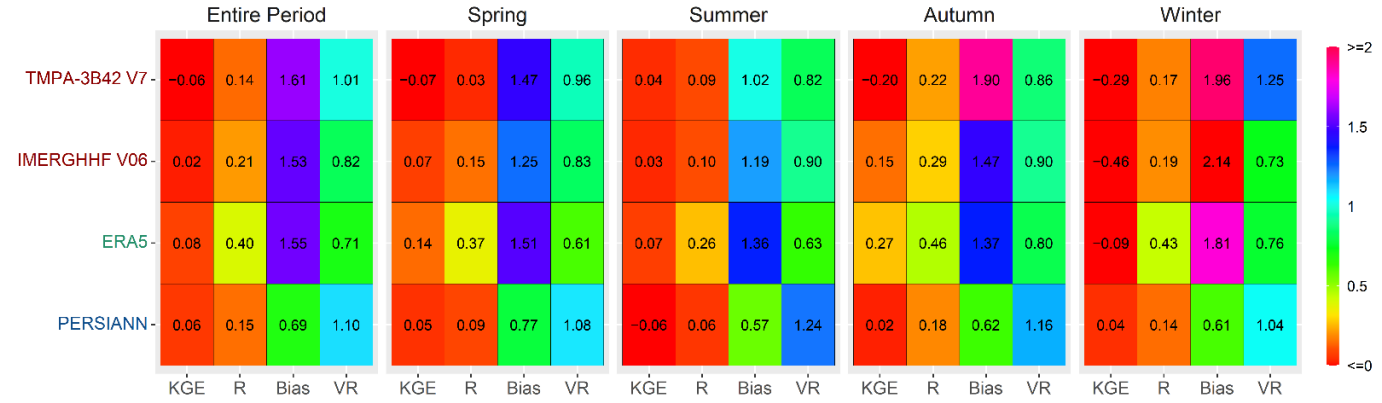

Figure 3. PPs' reliability at the regional scale under the Kling–Gupta efficiency (KGE) and its components for daily precipitation considering the entire period and four seasons. Y-axis color presents: satellite (blue), gauge and satellite (red), and reanalysis (green).

Figure 4 presents the detectability strength of the selected PPs for five precipitation intensities, which is evaluated by the Hansen–Kuiper (HK) score, considering the entire period and four seasons. Generally, PPs show better detectability for low-intensity daily precipitation, and their detectability strength decreases by increasing precipitation intensities. Among PPs, ERA5 shows high detectability for precipitation less than 1 mm/day for the entire period, and this amount increases to 0.47 during the autumn season. Moreover, ERA5 presents better detectability for moderate precipitation overall. All PPs show higher detectability for moderate precipitation compared with light precipitation. IMERGHHFv06 shows higher detectability compared with TMPA-3B42v7 for precipitation less than 1 mm/day. PERSIANN performs weakly for capturing different precipitation events, comparatively.

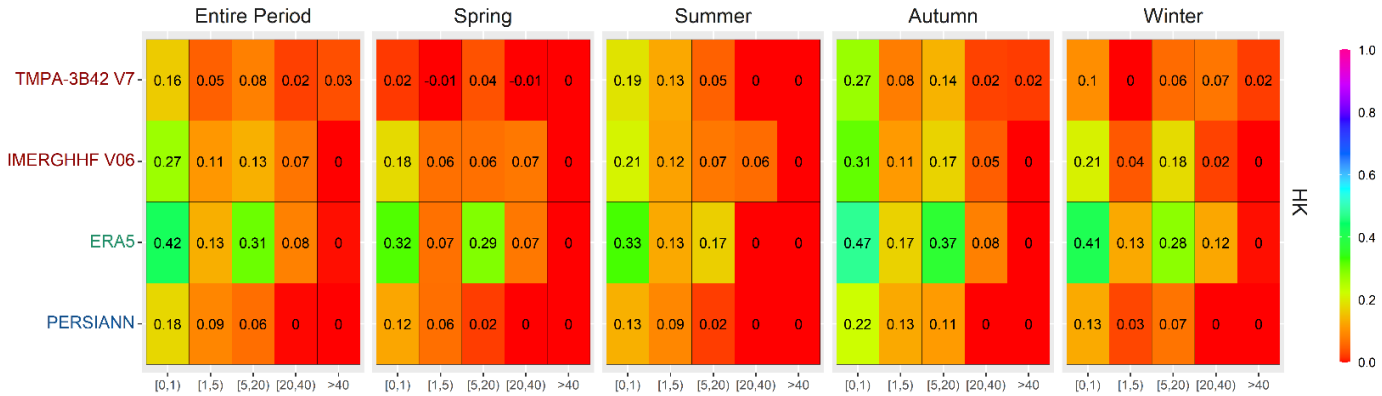

Figure 4. PPs' detection ability in reproducing daily precipitation intensities expressed in the form of the Hansen–Kuiper (HK) score, considering the entire period and four seasons. Y-axis color presents: satellite (blue), gauge and satellite (red), reanalysis (green).

3.3. Hydrologic Utility of PPs

Figure 5 displays the observed and simulated hydrographs in two schemes, including gauge precipitation and PPs for Karasu basin. Daily streamflows are reproduced by the TUW model for 5 water years classified into two parts: model calibration (October 2014 to September 2016) and validation (October 2016 to September 2019). Figure 6 maps the performance of PPs for streamflow simulation at the Karasu basin outlet. The model displays high performance using gauge observations in both the calibration and validation periods. On the other hand, PPs do not show the same success in scheme-1, although having high correlation ratios and high bias. Only PERSIANN indicates an unusual behavior with low calibration and high validation simulation. Furthermore, when the model parameters

are calibrated by each PP individually, all PPs show high reproducibility of streamflow for the calibration period and acceptable ranges for validation. For scheme-2, PERSIANN again performs unexpectedly, exhibiting the lowest results of all PPs. Table 3 summarizes TUW model parameter ranges and calibration results for observed precipitation and PPs.

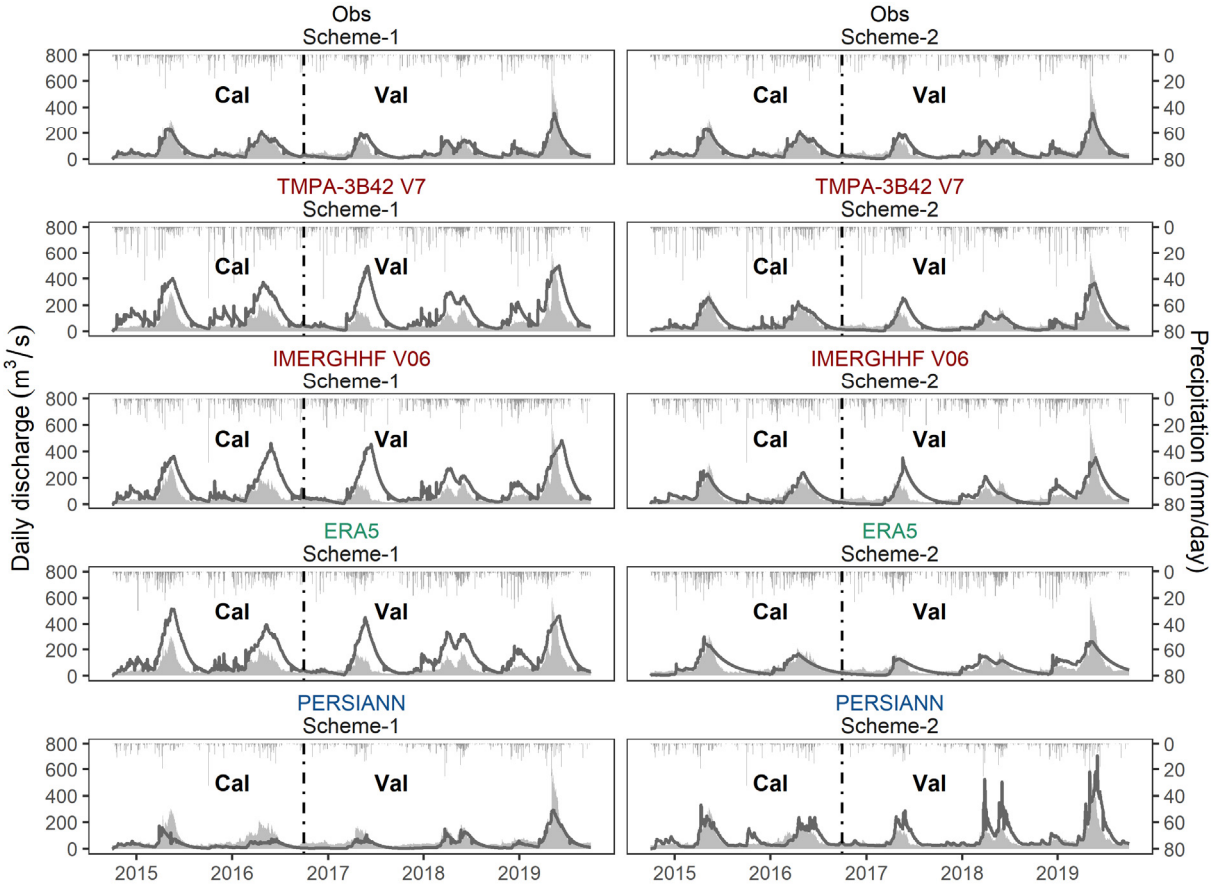

Figure 5. Hydrographs of observed and simulated daily discharge based on observed precipitation and four PPs for the calibration (October 2014 to September 2016) and validation (October 2016 to September 2019) periods in two schemes.

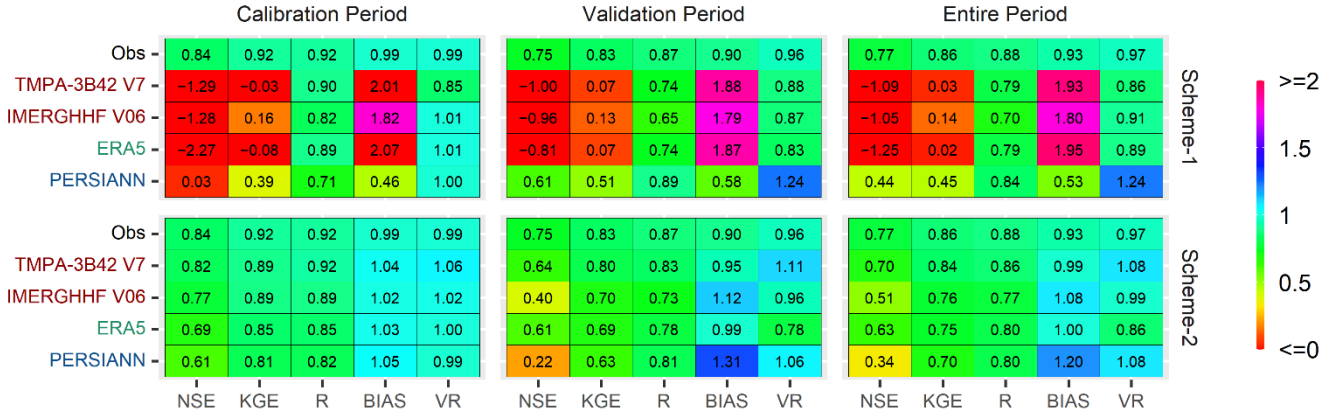

Figure 6. Performance of daily streamflow for observed precipitation and selected PPs. Y-axis color presents: satellite (blue), gauge and satellite (red), Reanalysis (green) and gauge (black).

4. Conclusions

In this study, the reliability of four PPs (TMPA-3B42v7, IMERGHHFv06, ERA5, and PERSIANN) is tested by direct comparison of the PPs with observed precipitation obtained from 23 ground stations. Moreover, the hydrologic utility of each PP on runoff is evaluated for 5 water years (October 2014 to September 2019) at the mountainous Karasu basin. Several performance metrics (KGE, HK, and NSE) are considered for the meteorological and hydrological evaluation. The major conclusions are summarized as follows:

- All PPs show high detectability for low-intensity precipitation, where their detectability strength decreases for high-intensity precipitation for the considered entire period and four seasons. Furthermore, ERA5 shows high detectability in almost all precipitation events compared with the other PPs.
- In the direct comparison, all PP performances (median of KGE varies from −0.06 of TMPA-3B42v7 to 0.08 of ERA5) are low for daily precipitation during the entire period. Although PP correlations (R) are higher, high/low bias and variability ratios cause detrimental effects.
- PPs show better reproducibility for streamflow when evaluated against direct precipitation comparison with gauge data. Moreover, PPs are able to estimate streamflow with high accuracy if model parameters are calibrated by PPs individually. TMPA-3B42v7 shows the highest performance for streamflow simulation in both the calibration (NSE, 0.82) and validation (NSE, 0.64) periods in scheme-2, followed by IMERGHHFv06 and ERA5. PERSIANN shows variable performance in both schemes for calibration/validation and has the lowest performance of all PPs in scheme-2.

Future work will include more PPs for direct precipitation comparison and hydrologic simulations.

Data Availability Statement: Publicly available datasets were analyzed in this study.

Conflicts of Interest: The authors declare no conflict of interest.

References

1. Zhang, Y.; Sun, A.; Sun, H.; Gui, D.; Xue, J.; Liao, W.; Yan, D.; Zhao, N.; Zeng, X. Error adjustment of TMPA satellite precipitation estimates and assessment of their hydrological utility in the middle and upper Yangtze River Basin, China. *Atmos. Res.* **2019**, *216*, 52–64. [CrossRef]
2. Indu, J.; Kumar, D.N. Copula-based modeling of TMI brightness temperature with rainfall type. *IEEE Trans. Geosci. Remote Sens.* **2013**, *52*, 4832–4845. [CrossRef]
3. Talchabhadel, R.; Aryal, A.; Kawaike, K.; Yamanoi, K.; Nakagawa, H.; Bhatta, B.; Karki, S.; Thapa, B.R. Evaluation of precipitation elasticity using precipitation data from ground and satellite-based estimates and watershed modeling in Western Nepal. *J. Hydrol. Reg. Stud.* **2021**, *33*, 100768. [CrossRef]
4. Berg, P.; Norin, L.; Olsson, J. Creation of a high resolution precipitation data set by merging gridded gauge data and radar observations for Sweden. *J. Hydrol.* **2016**, *541*, 6–13. [CrossRef]
5. Shi, H.; Chen, J.; Li, T.; Wang, G. A new method for estimation of spatially distributed rainfall through merging satellite observations, raingauge records, and terrain digital elevation model data. *J. Hydro-Environ. Res.* **2017**. [CrossRef]
6. Jeffrey, S.J.; Carter, J.O.; Moodie, K.B.; Beswick, A.R. Using spatial interpolation to construct a comprehensive archive of Australian climate data. *Environ. Model. Softw.* **2001**, *16*, 309–330. [CrossRef]
7. Li, M.; Shao, Q. An improved statistical approach to merge satellite rainfall estimates and raingauge data. *J. Hydrol.* **2010**, *385*, 51–64. [CrossRef]
8. Gourley, J.J.; Vieux, B.E. A method for identifying sources of model uncertainty in rainfall-runoff simulations. *J. Hydrol.* **2006**, *327*, 68–80. [CrossRef]
9. Xue, X.; Hong, Y.; Limaye, A.S.; Gourley, J.J.; Huffman, G.J.; Khan, S.I.; Dorji, C.; Chen, S. Statistical and hydrological evaluation of TRMM-based Multi-satellite Precipitation Analysis over the Wangchu Basin of Bhutan: Are the latest satellite precipitation products 3B42V7 ready for use in ungauged basins? *J. Hydrol.* **2013**, *499*, 91–99. [CrossRef]
10. Le, M.-H.; Lakshmi, V.; Bolten, J.; Du Bui, D. Adequacy of satellite-derived precipitation estimate for hydrological modeling in Vietnam Basins. *J. Hydrol.* **2020**, *586*, 124820. [CrossRef]
11. Li, X.; Chen, S.; Liang, Z.; Huang, C.; Li, Z.; Hu, B. Performance Assessment of GSMaP and GPM IMERG Products during Typhoon Mangkhut. *Atmosphere* **2021**, *12*, 134. [CrossRef]

12. Aznarez, C.; Jimeno-Sáez, P.; López-Ballesteros, A.; Pacheco, J.P.; Senent-Aparicio, J. Analysing the Impact of Climate Change on Hydrological Ecosystem Services in Laguna del Sauce (Uruguay) Using the SWAT Model and Remote Sensing Data. *Remote Sens.* **2021**, *13*, 2014. [CrossRef]
13. Doddy Clarke, E.; Griffin, S.; McDermott, F.; Monteiro Correia, J.; Sweeney, C. Which Reanalysis Dataset Should We Use for Renewable Energy Analysis in Ireland? *Atmosphere* **2021**, *12*, 624. [CrossRef]
14. Huffman, G.J.; Adler, R.F.; Bolvin, D.T.; Nelkin, E.J. The TRMM multi-satellite precipitation analysis (TMPA). In *Satellite Rainfall Applications for Surface Hydrology*; Springer: Berlin/Heidelberg, Germany, 2010; pp. 3–22.
15. Huffman, G.J.; Bolvin, D.T.; Braithwaite, D.; Hsu, K.-L.; Joyce, R.J.; Kidd, C.; Nelkin, E.J.; Sorooshian, S.; Stocker, E.F.; Tan, J. Integrated Multi-satellite Retrievals for the Global Precipitation Measurement (GPM) Mission (IMERG). In *Satellite Precipitation Measurement*; Springer: Berlin/Heidelberg, Germany, 2020; pp. 343–353.
16. Hersbach, H.; Dee, D. *ERA5 Reanalysis Is in Production*; ECMWF: Reading, UK, 2016; Volume 147. Available online: www.ecmwf.int/sites/default/files/elibrary/2016/16299newsletterno147spring2016.pdf (accessed on 16 July 2021).
17. Hsu, K.L.; Gupta, H.V.; Gao, X.; Sorooshian, S. Estimation of physical variables from multichannel remotely sensed imagery using a neural network: Application to rainfall estimation. *Water Resour. Res.* **1999**, *35*, 1605–1618. [CrossRef]
18. Nguyen, H.H.; Recknagel, F.; Meyer, W.; Frizenschaf, J.; Ying, H.; Gibbs, M.S. Comparison of the alternative models SOURCE and SWAT for predicting catchment streamflow, sediment and nutrient loads under the effect of land use changes. *Sci. Total Environ.* **2019**, *662*, 254–265. [CrossRef] [PubMed]
19. Singh, V.P. Hydrologic modeling: Progress and future directions. *Geosci. Lett.* **2018**, *5*, 15. [CrossRef]
20. Krysanova, V.; Srinivasan, R. Assessment of climate and land use change impacts with SWAT. *Reg. Environ. Chang.* **2015**, *15*, 431–434. [CrossRef]
21. Ghorbanpour, A.K.; Hessels, T.; Moghim, S.; Afshar, A. Comparison and assessment of spatial downscaling methods for enhancing the accuracy of satellite-based precipitation over Lake Urmia Basin. *J. Hydrol.* **2021**, *596*, 126055. [CrossRef]
22. Zhao, N. An Efficient Downscaling Scheme for High-Resolution Precipitation Estimates over a High Mountainous Watershed. *Remote Sens.* **2021**, *13*, 234. [CrossRef]
23. Wang, W.; Lin, H.; Chen, N.; Chen, Z. Evaluation of multi-source precipitation products over the Yangtze River Basin. *Atmos. Res.* **2021**, *249*, 105287. [CrossRef]
24. Aksu, H.; Akgül, M.A. Performance evaluation of CHIRPS satellite precipitation estimates over Turkey. *Theor. Appl. Climatol.* **2020**, *142*, 71–84. [CrossRef]
25. Amjad, M.; Yilmaz, M.T.; Yucel, I.; Yilmaz, K.K. Performance evaluation of satellite-and model-based precipitation products over varying climate and complex topography. *J. Hydrol.* **2020**, *584*, 124707. [CrossRef]
26. Irvem, A.; Ozbuldu, M. Evaluation of Satellite and Reanalysis Precipitation Products Using GIS for All Basins in Turkey. *Adv. Meteorol.* **2019**, *2019*, 4820136. [CrossRef]
27. Gupta, H.V.; Kling, H.; Yilmaz, K.K.; Martinez, G.F. Decomposition of the mean squared error and NSE performance criteria: Implications for improving hydrological modelling. *J. Hydrol.* **2009**, *377*, 80–91. [CrossRef]
28. Kling, H.; Fuchs, M.; Paulin, M. Runoff conditions in the upper Danube basin under an ensemble of climate change scenarios. *J. Hydrol.* **2012**, *424*, 264–277. [CrossRef]
29. WMO (World Meteorological Organization). *Guide to Hydrological Practices. Volume I: Hydrology—From Measurement to Hydrological Information*; WMO: Geneva, Switzerland, 2008. [CrossRef]
30. Zambrano-Bigiarini, M.; Nauditt, A.; Birkel, C.; Verbist, K.; Ribbe, L. Temporal and spatial evaluation of satellite-based rainfall estimates across the complex topographical and climatic gradients of Chile. *Hydrol. Earth Syst. Sci.* **2017**, *21*, 1295. [CrossRef]